The Reflection Grating Spectrometer on board *XMM-Newton*: status of the calibrations

J.W. den Herder [a]

[a]SRON, National Institute for Space Research, Sorbonnelaan 2, 3584 CA Utrecht, The Netherlands

The ESA X-ray Multi Mirror mission, *XMM-Newton*, carries two identical Reflection Grating Spectrometers (RGS) behind two of its three nested sets of Wolter I type mirrors. The instrument allows for high-resolution ($E/\Delta E$ = 100 to 600) measurements in the soft X-ray range (6 to 38 Å or 0.3 to 2.1 keV) with a maximum total effective area of about 140 cm^2 at 15 Å. Its design is optimized for the detection of the K-shell transitions of carbon, nitrogen, oxygen, neon, magnesium and silicon as well as the L-shell transitions of iron. After a short introduction to the instrument design and modes, this paper describes the status of the calibrations including the line spread function, the wavelength scale, the effective area and the instrumental background. It also addresses the stability of the response over the mission duration.

1. Introduction

The RGS design is illustrated in Fig. 1. Each instrument includes an array of reflection gratings placed in the converging beam at the exit of the X-ray telescope. The grating array reflects roughly half of the X-ray light to a strip of CCD detectors. The reflection grating arrays contain 181 and 182 gratings respectively. These are mounted at grazing incidence to the beam in the in-plane classical configuration in which the incident and diffracted rays lie in a plane perpendicular to the grating grooves. The diffraction efficiency ($\approx$ 10 %) is optimized for 15 Å. At the spectral focus, which is offset from the telescope center, an array of 9 back-illuminated CCDs is operated in frame transfer mode. The read-out times allow for the detection of single photons. Overlapping orders from the gratings can be separated using the CCD energy resolution. Full details of this design are given in [1] and [2].

Three operating modes are available with the RGS: Spectroscopy, High Time Resolution mode and Diagnostic mode. In the most commonly used mode (Spectroscopy) the CCDs are read-out sequentially with a read-out time per CCD of about 0.6 s. In this mode the CCD pulse height and the position of the photon along the dispersion axis and perpendicular to this axis are stored. This allows for optimal separation of source and background and therefore optimal S/N ratios. In the High Time Resolution mode the read-out time is reduced to about 15 ms per CCD at the expense of the cross dispersion data. In diagnostic mode full CCD images are transfered to the ground, allowing for a detailed study of the CCD performance.

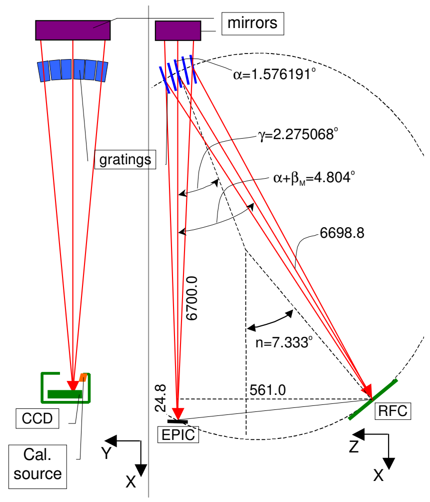

Figure 1. *Optical design of RGS (not to scale). X-rays are indicated by red lines entering from the top.*

2. Line spread function

The line spread function (LSF) matches very well the pre-flight expectations. This is illustrated in Fig. 2 where the modeled and the measured LSF are shown for a strong emission line of HR 1099. The predicted LSF is a convolution of the mirror response, the grating response and the CCD response taking into account the appropriate data selections (see [3] for details). In Fig. 3 the full width half maximum is shown for the two RGS instruments as a function of wavelength. The resolution varies typically between 100 and 600 (E/ΔE) in the first order and is about a factor 2 better in the second order.

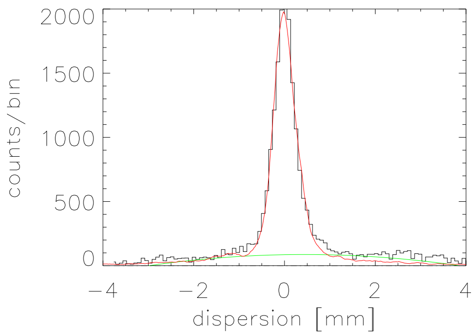

Figure 2. *Measured (black) and modeled LSF (red) for the O VIII Lyα line in HR 1099. The assumed background is indicated in green.*

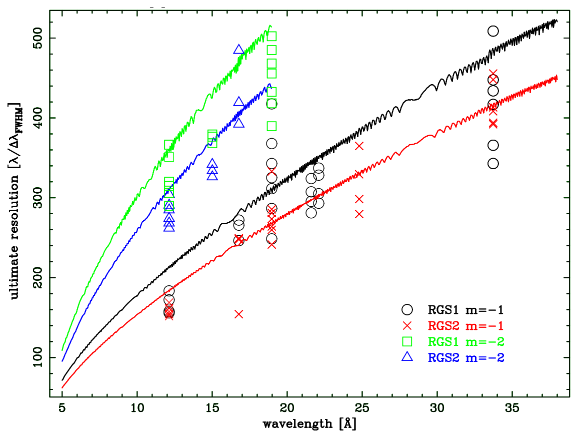

Figure 3. *Predicted (lines) and measured (points) FWHM for RGS1 and RGS2.*

3. Wavelength calibration

The wavelength scale is determined by the relative alignment of the instrument units (mirrors, gratings and detector). Using a set of strong emission lines from coronal sources, the accuracy of the wavelength-scale, fixed during the ground calibration, was determined to be 8 mÅ rms (1 σ). This is illustrated in Fig. 4 where the distribution of the difference between the measured and the expected wavelength is given for a number of well known emission lines. The typical spread is 7 to 8 mÅ (the data were collected at a regular intervals during the mission) Detailed analysis indicates that there are two main contributions to this spread: some 5 mÅ can be attributed to the satellite pointing and a similar amount to the detector geometry. It is expected that these numbers can be reduced somewhat and an accuracy of 4 mÅ is within reach.

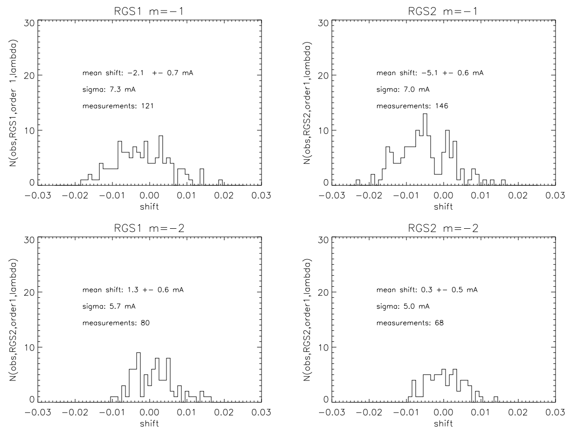

Figure 4. *Distribution of the difference between the measured and theoretical wavelength for 7 emission lines in 3 stars.*

4. Effective area

The effective area was calibrated on ground. Part of these calibrations included extensive unit calibrations. These unit calibrations were complemented by an end-to-end calibration campaign in the Panter facility in Munich. However, due to the finite source distance, the units had to be aligned differently and as result the end-to-end calibration is not fully representative for the flight configuration. Based on these ground calibrations a detailed model for the instrument effective area was optimized, taking into account the relevant physical processes. In orbit this model has been verified on a number of sources with relatively smooth continuum spectra. During this verification it became apparent that the detector includes a significant Oxygen absorption feature. This is illustrated in Fig. 5 where the spectrum for the combined data of two BL Lac objects with low extinction are shown (172 ks for Mrk 421 and 346 ks for PKS 2155-304) as well as the expected Interstellar Medium (ISM) extinction. There is a clear mismatch. Comparing these data with sources with high extinction (Sco X-1) it is possible to deduce the instrumental response over the O-edge. The result is shown in Fig.6 (see [4] for details). In the real data the sharp features will be convolved with the broader instrument response. The amount of Oxygen (in the form of ice or oxidized layers) is somewhat larger than expected. Applying this instrumental correction to the low extinction data improves the description considerably (see dashed curve in Fig. 5). The feature at 22.77 Å visible in this figure is not present in a number of other spectra (Sco X-1, 4U 0614+19) and has therefore an astrophysical origin.

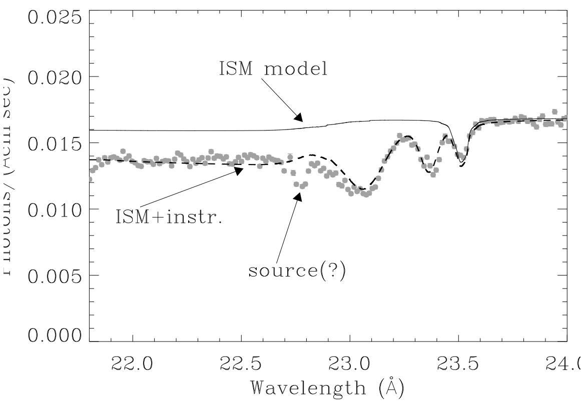

Figure 5. *Combined spectrum around the O-edge for Mrk 421 and PKS 2155-304 with the expected absorption from the ISM alone (solid line) and in combination with the the instrumental component (dashed).*

In addition we have verified the stability of the instrument response over time by repeated observations of the BL Lac object Mrk 421. This is illustrated in Fig. 7 where we display the difference

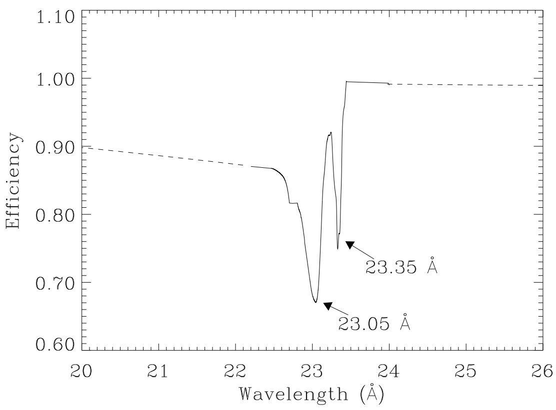

Figure 6. *Instrumental efficiency around the O-edge*

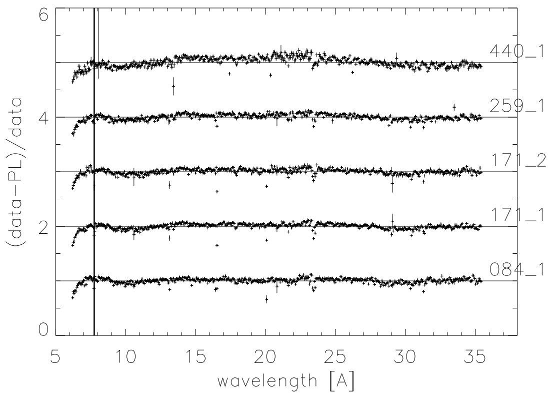

Figure 7. *Difference between the model (power law) and the data for observations of Mrk 421 at different orbits (indicated at the right).*

between the data, fitted by a power law spectrum with free index and normalization, for different orbits. Except for a small difference around the F-edge, and the absorption due to the 1s-2p transition in the ISM, the data are very well described by a power law spectrum for all periods. The RGS1 instrument returns in average a 3 % higher flux than RGS2. As is shown in this figure the effective area below 7 Å , where the effective area also drops steeply, is less well calibrated. Variations above 7 Å are of the order of 5 %. After corrections for these variations the remaining differences between RGS1 and RGS2 at the scale of a resolution element are about 2.5 %.

In Fig. 8 the RGS effective area is shown.

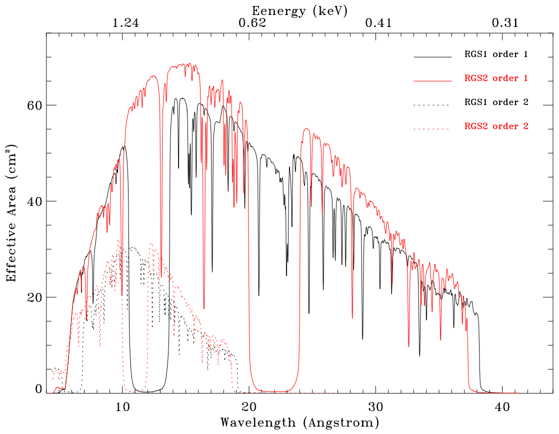

Figure 8. *Effective area for RGS1 and RGS2 (two orders)*

Apart of the two failing chains (CCD4 in RGS2 and CCD7 in RGS1) the CCD boundaries can be easily identified. Also the effect of hot pixels and columns is taken into account in this figure.

5. Background

RGS background includes the particle background, the diffuse X-ray background, internal fluorescence lines in the instrument, soft protons entering through the telescope and a component due to electronic noise. After excluding periods with high background due to soft protons, the background is reasonably stable. The typical background is shown in Fig. 9 where the background is integrated over the full cross dispersion direction but photons outside the CCD energy selection for a given dispersion angle are rejected. This background may vary up to 50 %. This background estimate can be used for extended sources. For point sources it is preferred to select an off-axis position in the cross dispersion direction and to use this as background.

6. In-orbit performance

The detectors degrade due to radiation damage. In addition a slow build up of contaminants (ice, hydro-carbons) may affect the effective area. In Fig. 10 the intensity of the on-board calibration sources is shown as a function of orbit. A slow decline is expected as the fluorescence radiation is generated by α particles from radioactive source (Cm^{244}) hitting a Teflon or Al target. The reduction of the countrate is somewhat faster than expected and this is attributed to tiny amounts of ice that stop the α particles before they hit the fluoresence target but that has no significant influence on the X-rays. The difference in the relative intensity between F and Al puts constraints on the maximum amount of ice/water.

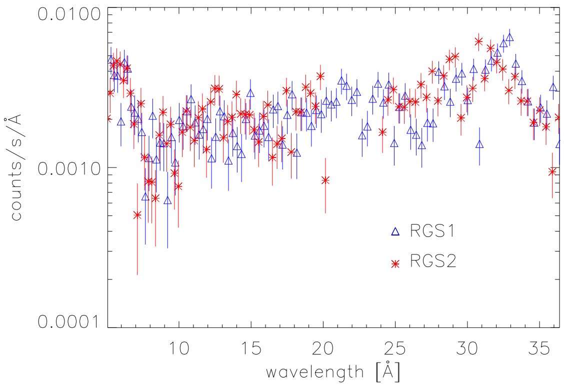

Figure 9. *RGS background*

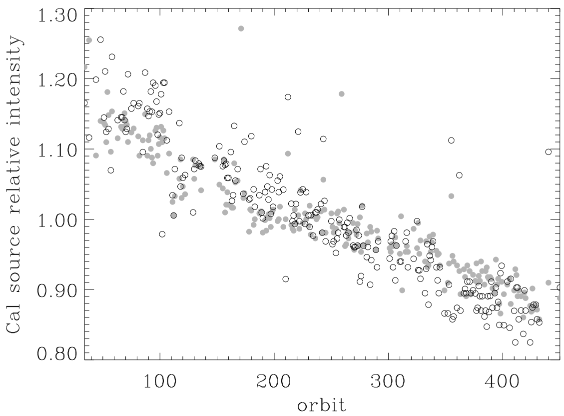

Figure 10. *Intensity of the calibration source for F-K (open circles) and Al-K (gray)*

Radiation damage of the CCDs includes the generation of trapping sites in the detectors as well as sites with increased dark current. As result of the trapping sites some charge can be lost when the charge is transfered over such a defect. This translates into a charge transfer inefficiency. Fig. 11 shows that the measured pulse height of the on-board calibration source is reduced by about 1 % over about one year. For an average of 10^3 transfers of the charge this corresponds to a degradation of the CTI by 10^{-5} per transfer. The data points which do not follow the steady decrease can be explained by details of the relevant observation (e.g. mixing of the source position (off-axis) with the on-board calibration source).

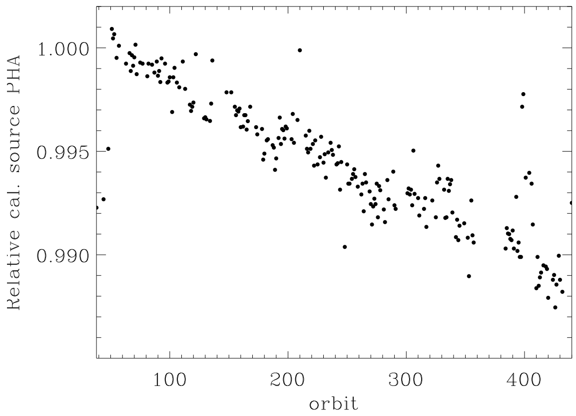

Figure 11. *Relative position of the on-board calibration source*

Pixels with an increased noise temperature have to be rejected as these distort the extracted spectra. These pixels can be easily identified by their frequency taking into account the shape of the LSF to ensure that the strong emission lines are not rejected. The result of this analysis is shown in Fig. 12. Detailed inspection of the data indicates that hot pixels come and go and the shown fluctuations are a true representation of the data. As it is expected that these hot pixels would be reduced by lowering the temperature of the CCDs, it is planned to reduce the operating temperature from −80°C to −110°C.

7. Conclusions

The RGS response is in good agreement with the predictions based on a realistic physical model of the instrument. The current wavelength accuracy (8 mÅ rms) can be improved by paying attention to the pointing and by using a modified instrumental geometry. Large scale variations in the effective area are typically about 5 % except

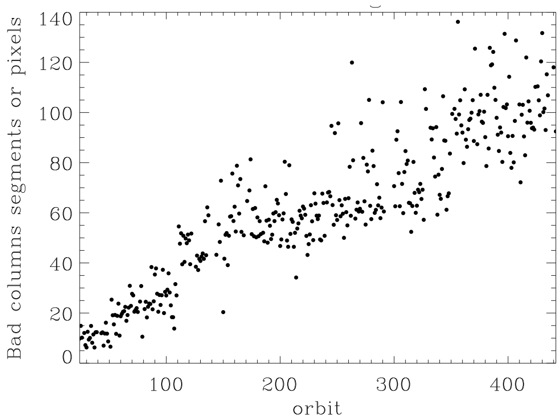

Figure 12. *number of rejected pixels due to increased noise*

below 7 Å where the difference is larger. Variations between RGS1 and RGS2 at the level of a resolution element are typically in the order of 2.5 % and this should be taken into account when weak absorption of emission features are analyzed.

To reduce the degradation of the instrument performance due to radiation damage, the instruments will be cooled from −80°C to −110°C in early November 2002.

REFERENCES

1. Herder, J.W.den, Brinkman, B., Kahn, S.M., et al., 2001, A&A 365, L7
2. Herder, J.W.den, Brinkman, B., Kahn, S.M., et al., 2002, SPIE 4851, in press
3. Herder, J.W.den, Brinkman, B., Kahn, S.M., et al., 2002, ESA SP-488, eds F.Jansen, in press
4. Vries, C.P. de, Herder, J.W. den, Kaastra, J.S., et al., 2003, submitted to A&A

ACKNOWLEDGEMENTS

XMM-Newton is an ESA science mission with instruments and contributions funded by ESA member states and the USA (NASA). The Reflection Grating Spectrometer has been developed as a collaborative effort between SRON, Columbmia University (USA), Mullard Space Science Laboratory (UK) and the Paul Sherrer Institute (Switzerland). The results presented in this paper have been produced by the instrument team.